Journal of Materials Chemistry A

ROYAL SOCIETY OF CHEMISTRY

PAPER

View Article Online
View Journal | View Issue

Cite this: J. Mater. Chem. A, 2021, 9, 281

A chemical map of NaSICON electrode materials for sodium-ion batteries†

Baltej Singh,‡[a] Ziliang Wang,‡[a] Sunkyu Park,[bcd] Gopalakrishnan Sai Gautam,[e] Jean-Noël Chotard,[bdg] Laurence Croguennec,[cdf] Dany Carlier,[cdf] Anthony K. Cheetham,[ag] Christian Masquelier[bdf] and Pieremanuele Canepa*[ah]

Na-ion batteries are promising devices for smart grids and electric vehicles due to the cost effectiveness arising from the overall abundance of sodium (Na) and its even geographical distribution. Among other factors, the energy density of Na-ion batteries is limited by the cathode electrode chemistry. NaSICON-based electrode materials are known for their wide range of electrochemical potentials, high ionic conductivity, and most importantly their structural and thermal stabilities. Using first-principles calculations, we chart the chemical space of 3d transition metal-based NaSICON phosphates with the formula $Na_xMM'(PO_4)_3$ (with M and M′ = Ti, V, Cr, Mn, Fe, Co and Ni) to analyze their thermodynamic stabilities and the intercalation voltages for Na^+ ions. Specifically, we compute the Na insertion voltages and related properties of 28 distinct NaSICON compositions. We investigate the thermodynamic stability of Na-intercalation in previously unreported $Na_xMn_2(PO_4)_3$ and $Na_xVCo(PO_4)_3$. The calculated quaternary phase diagrams of the Na–P–O–Co and Na–P–O–Ni chemical systems explain the origin of the suspected instability of Ni and Co-based NaSICON compositions. From our analysis, we are also able to rationalize anomalies in previously reported experimental data in this diverse and important chemical space.

Received 2nd November 2020
Accepted 21st November 2020

DOI: 10.1039/d0ta10688g

rsc.li/materials-a

1. Introduction

Developing new battery systems capable of storing increasing quantities of energy poses extraordinary scientific and economic challenges. Lithium (Li)-ion batteries power the world's portable devices, such as mobile phones, cameras, laptops, *etc.*, but the supply chains of Li and the required transition metals may soon be at risk due to geopolitical considerations.[1,2] Sodium (Na) appears to be a viable alternative to Li for battery applications due to its earth abundance, as well as the possibility of harvesting it directly from sea water. With Na being ~50 times more affordable compared to Li, Na-ion batteries (NIBs) are being explored by researchers worldwide, including a number of commercialization attempts.[3–8] In addition, inexpensive stainless-steel current collectors are typically used in NIBs instead of the expensive copper ones found in Li-ion cells.

Cathode materials factor prominently in the overall energy density stored by NIBs, and the optimization of electrode chemistries to provide high intercalation voltages and gravimetric/volumetric capacities remains a crucial aspect in the design of competitive NIBs. In theory, transition metal layered oxide-based cathode materials for NIBs would offer the largest theoretical energy densities.[5–7,9,10] However, the dominant two dimensional character of their structures strongly affects the longevity of the cathode material, with the electrochemical cell exhibiting a shorter-than-desired cycle life.[6,7,10–15] Promising alternatives to layered oxides are polyanion-based cathode materials.[16] Polyanion electrode materials leverage a combination of multivalent cations (*e.g.*, P^{5+}, Si^{4+} and S^{6+}) and anions (mostly O^{2-}) arranging into phosphate, silicate and sulfate (PO_4^{3-}, SiO_4^{4-} and SO_4^{2-}), which are thermodynamically stable by virtue of the strong binding energy of their polyanionic covalent bonds.[17–19]

[a]Department of Materials Science and Engineering, National University of Singapore, Singapore 117575, Singapore. E-mail: pcanepa@nus.edu.sg

[b]Laboratoire de Réactivité et de Chimie des Solides (LRCS), CNRS UMR 7314, Université de Picardie Jules Verne, 80039 Amiens Cedex, France. E-mail: christian.masquelier@u-picardie.fr

[c]CNRS, Univ. Bordeaux, Bordeaux INP, ICMCB, UMR CNRS 5026, F-33600, Pessac, France

[d]RS2E, Réseau Français sur le Stockage Electrochimique de l'Energie, FR CNRS 3459, F-80039 Amiens Cedex 1, France

[e]Department of Materials Engineering, Indian Institute of Science, Bengaluru, 560012, Karnataka, India

[f]ALISTORE-ERI European Research Institute, FR CNRS 3104, Amiens, F-80039 Cedex 1, France

[g]Materials Department and Materials Research Laboratory, University of California, Santa Barbara, California 93106, USA

[h]Chemical and Biomolecular Engineering, National University of Singapore, 4 Engineering Drive 4, Singapore, 117585

† Electronic supplementary information (ESI) available. See DOI: 10.1039/d0ta10688g

‡ These authors contributed equally.

An important class of phosphate electrodes discovered by Hong and Goodenough is the Natrium Super Ionic CONductors (NaSICONs),[20,21] with the formula $Na_xMM'(XO_4)_3$, where M and M′ are metals and X = Si, P and/or S. NaSICON electrode materials and electrolytes typically display significant Na^+-mobility.[22] The NaSICON framework is important for the development of new NIB materials,[17,22–29] since its structural tunability enables the exploration of a vast chemical space, which greatly diversifies the potential, electrochemical properties and related structural features. In theory, a charged $MM'(PO_4)_3$ NaSICON framework with redox-active transition metals M and M′ would allow the intercalation of up to 4 Na^+ ions,[9] which make these materials promising in terms of energy density.[30] Notwithstanding the challenges of working with carbon-based anodes in NIBs,[9,31–33] one could benefit from the presence of 4 Na^+ ions in NaSICONs, *e.g.*, $Na_4Mn^{II}V^{III}(PO_4)_3$.[34,35] However, the reversible extraction/intercalation of 4 Na^+ ions is yet to be reported in NaSICON frameworks.

As an example of a NaSICON cathode electrode, $Na_3V^{III}V^{III}(PO_4)_3$ (NVP) can reversibly exchange two electrons (*via* the activation of the V^{IV}/V^{III} redox couple) delivering $Na_1V^{IV}V^{IV}(PO_4)_3$ at an average voltage of ~3.4 V *vs.* Na/Na^+ with a capacity of ~110 mA h g^{-1} and an energy density of ~370 W h kg^{-1}.[27,36,37] One additional Na^+ can be inserted (electro)chemically into NVP to achieve $Na_4V^{II}V^{III}(PO_4)_3$ with a voltage of ~1.63 V *vs.* Na/Na^+. The reversible extraction of 3 Na^+ ions (*i.e.*, starting from $Na_4V^{II}V^{III}(PO_4)_3$ as the pristine material to $Na_1V^{IV}V^{IV}(PO_4)_3$ is possible but not practical due to the 1.8 V difference between the two processes (V^{IV}/V^{III} and V^{III}/V^{II}) and the difficult synthesis of $Na_4V_2(PO_4)_3$. Uebou *et al.*[38] demonstrated the extraction of ~2.5 Na^+ ions with partial reversibility.

Symmetric Na electrochemical cells entirely made of NaSICON frameworks adopt NVP as both the electrodes;[39] in the charged state of the battery the anode is $Na_4V^{III}V^{II}(PO_4)_3$ and the cathode is $Na_1V^{IV}V^{IV}(PO_4)_3$ with $Na_3Zr_2Si_2PO_{12}$ as the electrolyte. This could deliver an average voltage of ~1.8 V.[39–41] NVP suffers from poor intrinsic electronic conductivity due to the isolated VO_6 octahedra, which are never face-, edge- or corner-sharing with each other,[25,42] in contrast to their arrangement in layered-oxide cathodes where edge-sharing exists between MO_6 moieties.[6,9]

The Ti analogue of NVP is the Ti^{IV}-containing $NaTi^{IV}Ti^{IV}(PO_4)_3$ composition, which is stable in air and can reversibly exchange two electrons by benefitting from the Ti^{IV}/Ti^{III} redox couple, but at a lower voltage of ~2.1 V *vs.* Na/Na^+ compared to that of ~3.4 V for V^{IV}/V^{III} redox in NVP.[25,26] $NaTi^{IV}Ti^{IV}(PO_4)_3$ is also commonly used as a negative electrode material.[28] The NaSICON $Na_3Fe^{III}Fe^{III}(PO_4)_3$ exhibits a voltage–composition plateau at ~2.5 V *vs.* Na/Na^+ with a discharge capacity of ~61 mA h g^{-1} and is associated with the redox couple Fe^{III}/Fe^{II}.[43] The Fe^{IV}/Fe^{III} redox couple was claimed to be observed in $Na_3Fe^{III}Fe^{III}(PO_4)_3$ at ~3.4 V *vs.* Na/Na^+, with a limited specific discharge capacity of ~22 mA h g^{-1}.[44] Nevertheless, the formation of tetravalent iron ions has not yet been reproduced.

Yamada *et al.*[45] reported a voltage of ~4.5 V *vs.* Na/Na^+ (enabled by the reversible Cr^{IV}/Cr^{III} redox couple) when Na^+ is extracted from $Na_3Cr^{III}Cr^{III}(PO_4)_3$, which corresponds to the highest voltage ever reported among NaSICON materials with a single TM species. Importantly, the Mn, Co and Ni, $Na_xM_2(PO_4)_3$ NaSICON analogues have not yet been reported.

The high voltage delivered by the Cr^{IV}/Cr^{III} redox couple offers scope for exploring new high-voltage/capacity materials using more than one TM, *e.g.*, $Na_4Cr^{III}Mn^{II}(PO_4)_3$.[30,46] Other NaSICON materials, such as $Na_3V^{III}Cr^{III}(PO_4)_3$,[47] $Na_2Ti^{IV}V^{III}(PO_4)_3$,[48,49] $Na_3Ti^{IV}Mn^{II}(PO_4)_3$,[50,51] $Na_2Ti^{IV}Fe^{III}(PO_4)_3$,[52] $Na_4V^{III}Mn^{II}(PO_4)_3$,[34,35,53–56] $Na_3V^{III}Fe^{III}(PO_4)_3$ (ref. 29 and 35) and $Na_4V^{III}Ni^{II}(PO_4)_3$,[35] have also been studied to enable high reversible capacity and longevity as anode and cathode electrodes.

In general, to access three electrons (*i.e.*, 3 Na^+ ions per 2 TMs per formula unit) in any mixed TM NaSICON, two criteria must be met: (i) the TM must be in the +2 and +3 oxidation states in the fully discharged state (*i.e.*, 4 Na^+ ions) and (ii) at least one of the TMs must accommodate multiple redox active oxidation states. Compounds that meet these criteria are mainly either Mn or V-based NaSICONs, *e.g.*, $Na_2Ti^{IV}V^{III}(PO_4)_3$, $Na_3Ti^{IV}Mn^{II}(PO_4)_3$, $Na_4Mn^{II}V^{III}(PO_4)_3$, and $Na_4Cr^{III}Mn^{II}(PO_4)_3$, which undergo reversible electrochemical reactions up to three electrons with average voltages of ~2.4, ~3.2, ~3.4, and ~4.1 V *vs.* Na/Na^+. While $Na_4Cr^{III}Mn^{II}(PO_4)_3$ exhibits a high theoretical energy density (566 W h kg^{-1}) for a gravimetric capacity of 160 mA h g^{-1},[30] only ~40 mA h g^{-1} was reported at voltages below 1.6 V *vs.* Na/Na^+.

However, there remains a wide chemical space yet to be explored, which could yield new combinations of TMs enabling improved NaSICON electrode materials. A systematic study, either experimental or theoretical, of trends in voltages and the phase behavior of possible transition-metal combinations within NaSICON electrode materials has not yet been reported.

We present a first-principles study that charts the chemical space of 28 different $Na_xMM'(PO_4)_3$-electrode chemistries, where M and M′ can be any of the 3d TM, Ti, V, Cr, Mn, Fe, Co and Ni, with the Na content varying in the range of $1 \leq x \leq 4$. We derive the intercalation voltages for all the 28 $Na_xMM'(PO_4)_3$ systems, validate our predictions with available experimental data, and identify promising NaSICON compositions to be targeted experimentally. We find new promising or not fully explored $Na_xMM'(PO_4)_3$ compositions, *e.g.*, $Na_xMn_2(PO_4)_3$ ($1 \leq x \leq 4$), $Na_xCo_2(PO_4)_3$ ($3 \leq x \leq 4$), $Na_xTiCo(PO_4)_3$ ($2 \leq x \leq 4$), $Na_xVCo(PO_4)_3$ ($1 \leq x \leq 4$), $Na_xCrCo(PO_4)_3$ ($2 \leq x \leq 4$), $Na_xCoMn(PO_4)_3$ ($2 \leq x \leq 4$) and $Na_xCrFe(PO_4)_3$ ($2 \leq x \leq 4$). We analyze the possible origins of the difficulties in synthesizing specific NaSICON chemistries.

2. Results

2.1 Structural features of $Na_xMM'(PO_4)_3$ electrodes

Depending on the TM species, temperature and/or Na content (x) per formula unit (f.u.) NaSICON materials typically adopt a rhombohedral ($R\bar{3}c$),[45,57] an ordered monoclinic ($C2/c$ or Cc),[20,21,47] or, in the specific case of α-$Na_3Ti^{III}Ti^{III}(PO_4)_3$,

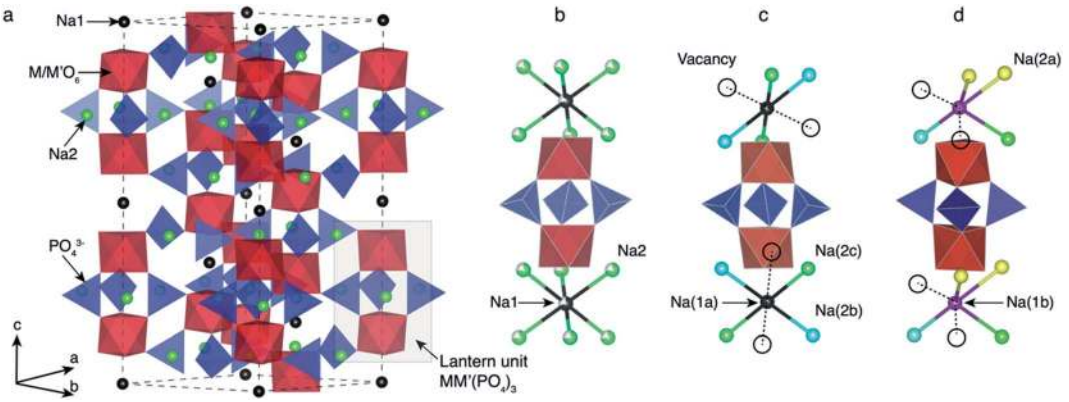

Fig. 1 (a) The rhombohedral ($R\bar{3}c$) structure of $Na_4MM'(PO_4)_3$ with M and M′ = Ti, V, Cr, Mn, Fe, Co and Ni. The "lantern unit" is made up of two MO_6 (or $M'O_6$) octahedra (red) sharing corners with PO_4^{3-} tetrahedra (blue). The gray box in (a) highlights the arrangement of the lantern units. Two distinct Na ions, *i.e.*, Na1 (black) and Na2 (green), are present in the rhombohedral NaSICONs. Panel (b) shows the lantern representation of the Na disordering (with partial Na occupancies on Na1 and Na2 sites) in the rhombohedral $Na_3MM'(PO_4)_3$ polymorph. Panel (c) shows a local view (lantern unit) of the complete ordering of Na^+ ions in the corresponding $Na_3MM'(PO_4)_3$ monoclinic ($C2/c$) phase. Panel (d) shows the local environment of sites Na1b (violet) and Na2a (yellow) in the same monoclinic arrangement. Vacancies are represented by open circles.

a triclinic structure ($P1$).[58] For example, $Na_4V^{II}V^{III}(PO_4)_3$ and $Na_4Fe^{II}Fe^{III}(PO_4)_3$ (ref. 59) are rhombohedral, while $Na_3V^{III}V^{III}(PO_4)_3$,[57] $Na_3Fe^{III}Fe^{III}(PO_4)_3$,[43] $Na_3Ti^{III}Ti^{III}(PO_4)_3$ and $Na_3Cr^{III}Cr^{III}(PO_4)_3$ tend to form monoclinic[58] structures at room temperature due to Na/vacancy orderings. Fig. 1 shows the archetypal structure of the rhombohedral $Na_xMM'(PO_4)_3$.

$Na_xMM'(PO_4)_3$ materials consist of $(M, M')O_6$ octahedral and PO_4 tetrahedral units. As shown in Fig. 1, three PO_4 tetrahedra share all their corners with two $(M,M')O_6$ octahedra forming the "lantern units"—a recurrent motif of NaSICON structures. The lantern units assemble into a 3-D $MM'(PO_4)_3$ framework producing two types of available sites for Na in the rhombohedral phase (Fig. 1b): Na1 (one per f.u.) and Na2 (three per f.u.). The six-coordinated Na1 sites are located between two $(M,M')O_6$ octahedra, while the Na2 sites remain eight-coordinated with the O atoms of the PO_4 tetrahedra. At $x = 4$ in $Na_xMM'(PO_4)_3$, all the Na positions (*i.e.*, 1 × Na1 and 3 × Na2 per f.u.) are fully occupied and the structure is ordered and rhombohedral. In several NaSICONs, the Na^+ ions are fully ordered at $x = 3$ and the structure adopts monoclinic ($C2/c$) symmetry (Fig. 1c), where the Na1 site splits into two distinct sites (*i.e.*, fully occupied Na1a and Na1b). The Na2 site splits into five sites (3 fully occupied, Na2a, Na2b and Na2c, and 2 vacancies).

2.2 Na intercalation in $Na_xM_2(PO_4)_3$ NaSICONs

The energetics of Na intercalation and the corresponding average voltages (see Methodology in Section 5) for single TM (M = M′) NaSICON electrodes are shown in panels (a) and (b) of Fig. 2. The computed formation energies for the most stable orderings in $Na_xM_2(PO_4)_3$ are displayed in Fig. 2a as a function of Na concentration, where the lower energy envelopes form the so-called convex hull (solid lines) for a given $Na_xM_2(PO_4)_3$ system. The convex hull highlights the thermodynamic phase behavior at 0 K of Na (de)intercalation from/into the $Na_xM_2(PO_4)_3$ frameworks. Since the convex hull at 0 K does not include any entropic and pV effects, it informs on the propensity of Na to bond with the $M_2(PO_4)_3$ frameworks. Among the M = Ti, V, Cr, Mn, Fe, Co and Ni compounds, NaSICONs based on Ti, V, Cr and Fe have been reported experimentally.[28,36,43–45] From previous experimental work, the redox activities of Ti and V provide accessible Na concentrations ranging in $1 \leq x \leq 4$, while $Na_xCr_2(PO_4)_3$ spans a narrower range of Na concentration ($1 \leq x \leq 3$), being limited by the Cr^{IV}/Cr^{III} redox couple. Notably, the Cr^{III}/Cr^{II} redox couple has not been cycled reversibly in NaSICON frameworks so far.

The structures represented by specific Na/vacancy orderings falling above the convex hull are thermodynamically unstable/metastable and are shown in Fig. S1–S7 of the ESI.† Note that the unstable Na/vacancy orderings should decompose to the closest ground state(s) identified by the convex hulls in Fig. 2a. For example, in Fig. S2,† $Na_2V_2(PO_4)_3$ ($C2$) is found to be slightly metastable (~1.8 meV per atom above the stability line) and will phase separate into $Na_1V^{IV}V^{IV}(PO_4)_3$ and $Na_3V^{III}V^{III}(PO_4)_3$. Given the small metastability of $Na_2V_2(PO_4)_3$, we expect this compound to be stabilized by entropic effects. Consequently, the stable structures lying on the convex hull (*e.g.*, $Na_3V^{III}V^{III}(PO_4)_3$) give rise to a "step" in the calculated Na voltage curve (see Fig. S2†). The convexity, that is the depth of the convex hull, is an indication of the thermodynamic stabilities of the specific Na/vacancy configurations. The calculated ground states on the convex hull do not necessarily correspond to topotactic structures since we allow changes to the symmetry (*e.g.*, rhombohedral → monoclinic) of the host during deintercalation of Na from $Na_4MM'(PO_4)_3$ in our calculations.

Analyzing Fig. 2a and b, the following general trends can be deduced:

(i) The end member compositions in $Na_xM_2(PO_4)_3$, *i.e.*, $x = 1$ and 4, typically adopt the rhombohedral ($R\bar{3}c$ or $R\bar{3}$) space group. Exceptions to this trend are $Na_4Cr^{II}Cr^{III}(PO_4)_3$ and $Na_4Mn^{II}Mn^{III}(PO_4)_3$, which are predicted to have triclinic ($P\bar{1}$) symmetry probably due to Jahn–Teller distortions of high-spin

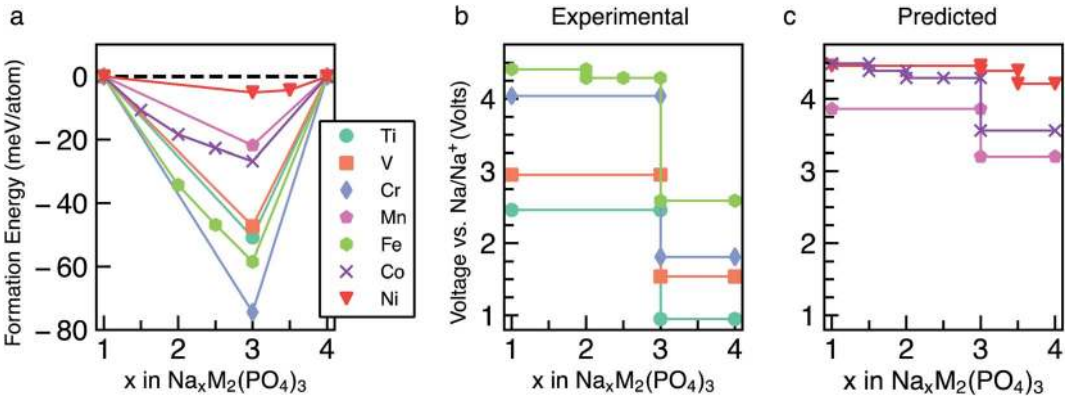

Fig. 2 Panel (a) shows the computed formation energies and respective convex hulls for Na vacancy orderings as a function of Na concentration (x) in $Na_xM_2(PO_4)_3$ where M = Ti, V, Cr, Mn, Fe, Co and Ni. Panels (b) and (c) show the intercalation voltages *vs.* Na/Na^+ for the experimentally known (M = Ti, V, Cr and Fe) and predicted (M = Mn, Co and Ni) $Na_xM_2(PO_4)_3$ compounds, respectively. Only the stable orderings forming the convex hull are displayed in panel (a). The energies of unstable configurations for each convex hull are shown in Fig. S1–S7 of the ESI.†

Cr^{2+} and Mn^{3+} d^4 ions. These have not yet been observed experimentally.

(ii) A global minimum in the formation energy curves is present across all transition-metal $Na_xM_2(PO_4)_3$ systems at $x = 3$ (Fig. 2a).[41]

(iii) Among all the $Na_3M^{III}M^{III}(PO_4)_3$ compounds investigated, $Na_3Cr^{III}Cr^{III}(PO_4)_3$ displays the deepest or lowest (*i.e.*, most favorable) formation energy, followed by $Na_3Fe^{III}Fe^{III}(PO_4)_3$ > $Na_3Ti^{III}Ti^{III}(PO_4)_3$ ≈ $Na_3V^{III}V^{III}(PO_4)_3$, respectively, which reflects the stability of the M^{3+} oxidation states of these TMs. The stability of $Na_3Cr^{III}Cr^{III}(PO_4)_3$ is enhanced by the large ligand field stabilization energy of the Cr^{3+} ($3d^3$) cation. The other compounds, $Na_3Co^{III}Co^{III}(PO_4)_3$, $Na_3Mn^{III}Mn^{III}(PO_4)_3$ and $Na_3Ni^{III}Ni^{III}(PO_4)_3$, display shallower (*i.e.*, less favorable) formation energies (<25 meV per atom, Fig. 2a). The shallow convex hulls for $Na_xMn_2(PO_4)_3$ and $Na_xNi_2(PO_4)_3$ are caused by the Mn^{3+} and Ni^{3+} ions which are both Jahn–Teller active. The magnetic moment of Co^{3+} $Na_3Co^{III}Co^{III}(PO_4)_3$ is ~3.0 μ_B, indicating an intermediate spin state and possible Jahn–Teller activity.

(iv) Unsurprisingly, the deep minima in the convex hull plot of Fig. 2a lead to a large voltage step as shown in Fig. 2b and d, following the sequence Cr > Fe > Ti > V > Co > Mn > Ni.

(v) The M(III/II) redox couples that correspond to Na contents from $x = 3$ to $x = 4$, follow the voltage trend Ni > Co > Mn > Fe > Cr > V > Ti, while the M(IV/III) couples ($x = 1$ to $x = 3$) follow the sequence Ni > Co > Fe > Cr > Mn > V > Ti. Thus, Ni and Co (V and Ti) display the highest (lowest) average voltages for both M redox couples.

To validate our methodology, we have benchmarked our results against experimental observations in $Na_xV_2(PO_4)_3$, which has been extensively studied.[57,60] Experimentally, $Na_3V^{III}V^{III}(PO_4)_3$ adopts monoclinic symmetry ($C2/c$) at room temperature, which is in qualitative agreement with our DFT calculations identifying the monoclinic ordering (Cc) as the stable structure at $x = 3$. From Fig. 2a, $Na_3V^{III}V^{III}(PO_4)_3$ is on the convex hull with $Na_1V^{IV}V^{IV}(PO_4)$ and $Na_4V^{II}V^{III}(PO_4)_3$, which adopt the rhombohedral space groups $R\bar{3}c$ and $R\bar{3}$, respectively; this is consistent with X-ray diffraction experiments.[36,57,61] In Fig. 2b, the extraction of 2 Na atoms from $Na_3V^{III}V^{III}(PO_4)_3$ gives rise to an average voltage of ~2.96 V *vs.* Na/Na^+ and corresponds to the V^{IV}/V^{III} redox couple, while the insertion of Na into $Na_3V^{III}V^{III}(PO_4)_3$ results in a voltage of 1.54 V (associated with the V^{III}/V^{II} redox couple). Experimentally, both the V redox couples (V^{IV}/V^{III} and V^{III}/V^{II}) are involved in two-phase reaction mechanisms, yielding average voltages of ~3.40 V and ~1.63 V *vs.* Na/Na^+, respectively,[60] which are in reasonable agreement with our computed values. Notably, both GGA+U and hybrid functionals underestimate the computed voltages of $Na_xV_2(PO_4)_3$ (see Section S2 in the ESI†). Another important assessment to verify the validity of our simulations is ensuring that changes in oxidation states of the TMs upon Na extraction/insertion are captured. We verify that the correct redox processes do occur in our calculations by tracking the on-site magnetic moments on the TM atoms (Table S1†), as well as the transition metal coordination environments (Table S2†), which are discussed in Section S3 of the ESI.†

Whenever we could not assign the expected oxidation state of the TMs directly from the computed magnetic moments (*e.g.*, in the cases of Fe, Co and Ni based NaSICONs), we inspected the density of states (DOS). Additional DOSs is are reported in Section S4 of the ESI (Fig. S9–S12).† As an example, we show in Fig. 3 the total and atom-projected DOS in $Na_xV_2(PO_4)_3$, for $x =$ 1, 3 and 4, which are the ground states identified in Fig. 2. The DOS is displayed for spin up and spin down states in the range of interest (−2.5 to 2 eV) around the Fermi energy. Unless a given structure is metallic, the top of the Fermi energy is arbitrarily set to the top of the valence band.

Panels (a) and (b) in Fig. 3 show the results for $Na_1V^{IV}V^{IV}(PO_4)_3$ and $Na_3V^{III}V^{III}(PO_4)_3$, respectively. From the projected DOS, the valence bands near the Fermi energy are occupied by 3d electrons of vanadium (red line), while the 2p O states (orange line) lie at lower energies. In general, the vanadium 3d states tend to dominate the valence band and shift at higher energies as more Na is inserted, closing the band gap (>1 eV for both compounds). The monoclinic distortion of

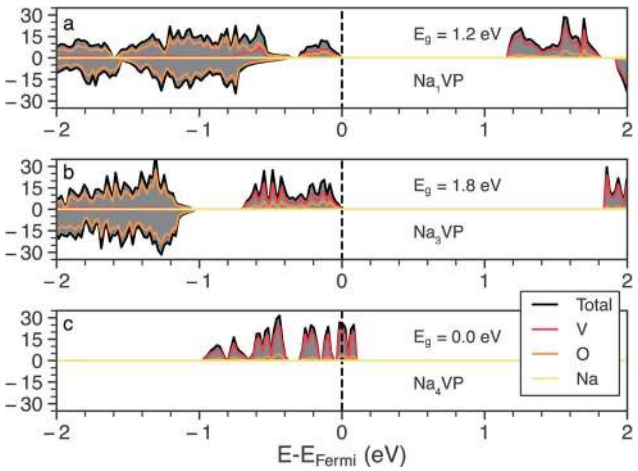

Fig. 3 The total (gray) and atom projected (V red, O orange and Na yellow) DOS of the $Na_xV_2(PO_4)_3$ NaSICON (NVP), where for Na concentrations $x = 1$ (panel a), 3 (panel b) and 4 (panel c). The vertical line denotes the Fermi energy level and E_g is the calculated band gap at the GGA+U level of theory.

$Na_3V^{III}V^{III}(PO_4)_3$ is responsible for an increase in the band gap (~1.8 eV) contrary to the Na = 1 and Na = 4 trends. As expected, the intercalation of more Na^+ ions as in $Na_4V^{III}V^{II}(PO_4)_3$ (Fig. 3c) further increases (destabilizes) the valence band, with this composition becoming gapless and showing a Fermi energy dominated by V(3d) states when GGA+U is used. For the $Na_4V^{III}V^{II}(PO_4)_3$, the band gap opens to ~0.3 eV when the more accurate HSE06 hybrid functional is used at the relaxed HSE06 structure. Very recent hybrid functional simulations on $Na_xTi_2(PO_4)_3$ have verified these orders of magnitude, with $Na_4Ti^{III}Ti^{II}(PO_4)_3$ showing a small band gap of ~0.59 eV.[62]

In the case of $Na_xNi_2(PO_4)_3$ the projected DOS of Fig. S12† suggests metallic behavior at all the Na concentrations explored (*i.e.*, $x = 1$, 3 and 4). $Na_xMn_2(PO_4)_3$ and $Na_xCo_2(PO_4)_3$ show band gaps > 1.0 eV at $x = 3$ and 4, but become metallic at $x = 1$, as shown in Fig. S9 and S11.† $Na_1Fe^{IV}Fe^{IV}(PO_4)_3$ also appears, surprisingly, metallic (Fig. S10†), which introduces difficulties in localizing the Fe^{III}/Fe^{IV} redox couple. Therefore, due to the apparent metallic behavior of some of these systems (Fe, Co and Ni-based NaSICONs), we were unable to assign unique oxidation states to their TMs. Notably, DFT is a ground state theory and not adequate in the prediction of accurate band gaps.[63]

2.3 Na^+ ion intercalation in $Na_xMM'(PO_4)_3$ NaSICON structures

We extend our analysis to the reversible extraction of Na from mixed $Na_4MM'(PO_4)_3$ compounds where, for the sake of simplicity, the ratio M : M′ is fixed as 1 : 1. While all the M : M′ combinations have been considered, to simplify our discussion we concentrate on the cases where M = Ti, while M′ = Ti, V, Cr, Mn, Fe, Co and Ni. Other mixed $Na_4MM'(PO_4)_3$ are reported in

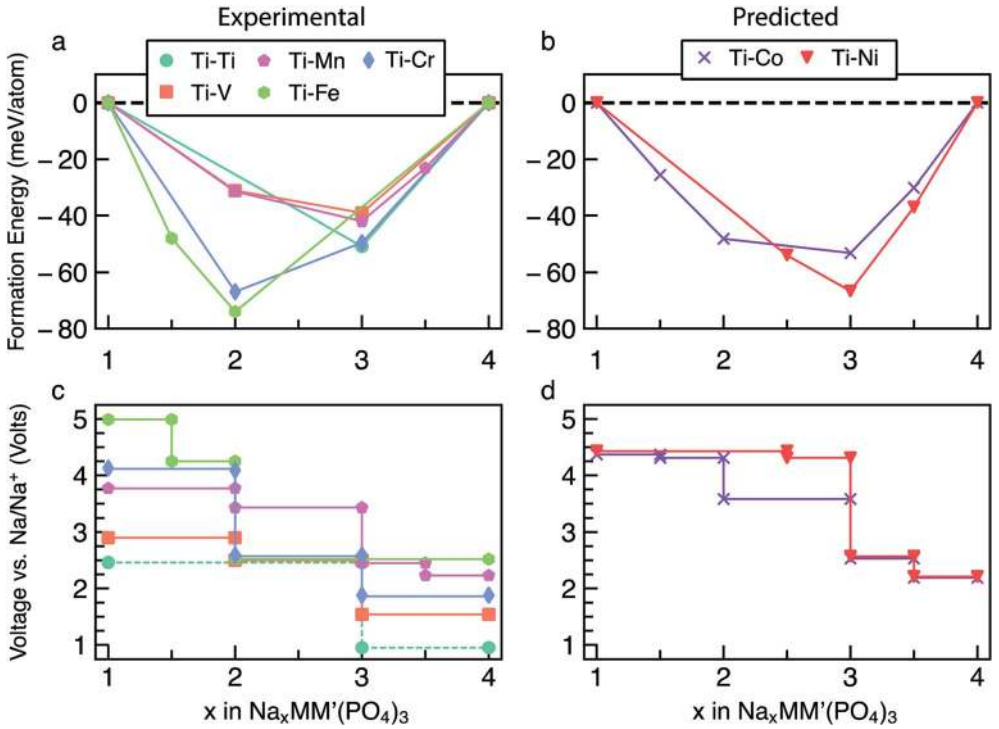

Fig. 4 Panels (a) and (b) show the computed convex hulls as a function of Na concentrations (x) for $Na_xTiM'(PO_4)_3$, where M′ = Ti, V, Cr, Mn, Fe in panel (a) and M′ = Co and Ni in panel (b). Panels (c) and (d) show the corresponding Na (de-)intercalation voltages over changes in the Na-content. The energies of unstable configurations for each convex hull, as well as complete voltage curves for each compound, are given in the ESI (Fig. S13–S33).† The symbols in panels (a) and (b) indicate stable ordered phases. To facilitate the visualization of the voltage curves near ~2.8 V *vs.* Na/Na^+ the Ti–Cr curve in panel (c) has been slightly lifted, but it is expected to overlap the Ti–V and Ti–Mn voltage curves.

Section S5 of the ESI (Fig. S13–S33).† The main reason behind choosing Ti-based mixed TM NaSICONs is their maximum experimental electrochemical data availability as compared to other combinations. Fig. 4a and b show the calculated convex hulls for experimentally reported and theoretical $Na_xTiM'(PO)$ compounds, with Na contents in the range $1 \leq x \leq 4$. Fig. 4c displays the corresponding voltages. $Na_xTi_2(PO_4)_3$ is also reported in Fig. 4a and c as a reference.

Among the $Na_xTiM'(PO_4)_3$ systems, only $Na_xTi_2(PO_4)_3$, $Na_xTiV(PO_4)_3$ and $Na_xTiMn(PO_4)_3$ have been experimentally investigated over the entire Na composition range ($1 \leq x \leq 4$),[28,48–51] while $Na_xTiCr(PO_4)_3$ (ref. 52 and 64) and $Na_xTiFe(PO_4)_3$ (ref. 52) have been studied in limited ranges of $1 \leq x \leq 3$ and $2 \leq x \leq 4$, respectively. $Na_xTiCo(PO_4)_3$ and $Na_xTiNi(PO_4)_3$ are theoretical compounds and have not yet been reported experimentally.

In general, the end member compositions at $x = 1$ and 4 (Fig. 4a and b) of the Ti–M′ NaSICON electrodes adopt rhombohedral symmetry ($R\bar{3}c$ or $R\bar{3}$, or $R32$) except for $Na_4Ti^{III}Cr^{II}(PO_4)_3$ ($P\bar{1}$) and $Na_1Ti^{IV}Fe^{IV}(PO_4)_3$ ($P1$), which are theoretically derived. This could be due to Jahn–Teller effects caused by the high-spin d^4 electronic configurations of Cr^{2+} and Fe^{4+}, respectively, as well as the low stability of Fe^{4+}. For $Na_xTiM'(PO_4)_3$ with M′ = V, Mn, Co and Ni, a global minimum in the convex hull is located at $x = 3$, and the magnitudes of the formation energy follow the trend Ni > Co > Mn > V. On the other hand, the global minima for the M′ = Ti, Cr and Fe NaSICONs are located at $x = 2$ (Fig. 4a), which is driven by the high stability of their stable oxidation states Ti^{4+}, Cr^{3+} and Fe^{3+}, respectively. Overall, the depth of the convex hulls (*i.e.*, maximum magnitude of formation energies) for mixed TM NaSICONs follows the trend Fe > Cr ∼ Ni > Co > Ti > Mn ∼ V.

Fig. 4c and d present the computed voltages for Na extraction from $Na_xTiM'(PO_4)_3$ in the composition range $1 \leq x \leq 4$. Expectedly, the compound exhibiting the lowest intercalation voltage (∼0.96 V) is $Na_xTi_2(PO_4)_3$ for $3 \leq x \leq 4$, which overestimates the experimental voltage (∼0.4 V) reported by Senguttuvan *et al.*[28] The DFT data of Fig. 4a suggest that an unreported stable phase appears at $Na_{1.5}TiFe(PO_4)_3$, but with an oxidation state for Fe of 3.5 (Fe^{IV} + Fe^{III}). Although the highest Na intercalation voltage (∼4.99 V) is computed for $Na_xTiFe(PO_4)_3$ between $x = 1.5$ and $x = 1$, the oxidation state of Fe would have to be +4, which may not be experimentally accessible in a reversible manner. We find that $Na_1Fe^{IV}Fe^{IV}(PO_4)_3$, where iron is expected to be Fe^{4+} appears metallic from the DOS in Fig. S10.†

To assess the quality of our computed data, we analyzed in detail the experimentally reported data for $Na_xTiV(PO_4)_3$. At $x =$ 1, 2 and 4, $Na_xTiV(PO_4)_3$ has rhombohedral symmetry ($R\bar{3}c$), while the structure of $Na_3TiV(PO_4)_3$ is monoclinic ($C2/c$).[48,49] Our calculations reproduce the rhombohedral symmetry ($R\bar{3}c$) at $x =$ 1 and 4 and the monoclinic symmetry (Cc) at $x = 3$, whereas we find a triclinic structure ($P\bar{1}$) for $Na_2TiV(PO_4)_3$.[48] The $Na_xTiV(PO_4)_3$ convex hull (Fig. 4a) displays a minimum at $x = 3$, analogous to the observed minima in the $Na_xM_2(PO_4)_3$ systems (Fig. 2a); this also provides the largest step in the corresponding voltage profile of Fig. 4c. In particular, the Na extraction from $Na_4Ti^{III}V^{II}(PO_4)_3$ takes place through the redox couples V^{III}/V^{II}

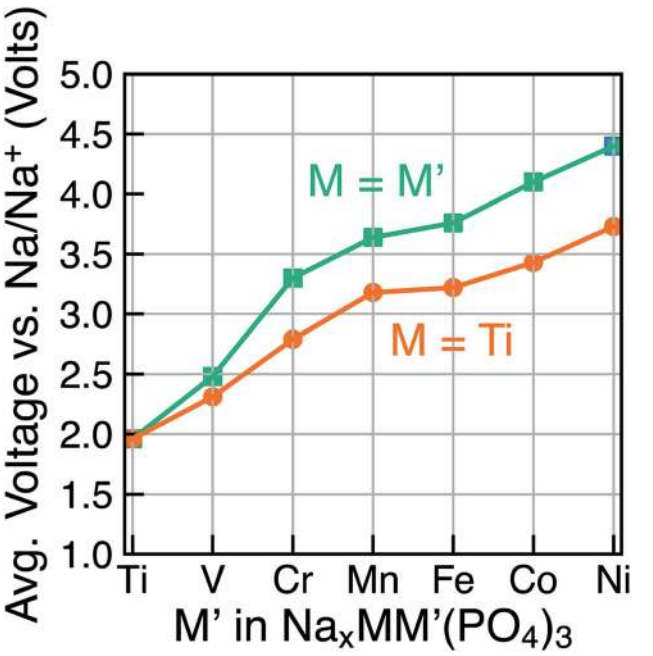

Fig. 5 The calculated average voltage per extracted Na^+ ion *vs.* Na/Na^+ over the *x* range[1–4] in $Na_xMM'(PO_4)_3$ compounds, where M = M′ (green) or M = Ti (orange) and M′ = V, Cr, Mn, Fe, Co and Ni.

1.54 V (experimentally ∼1.6 V [48,49]), Ti^{IV}/Ti^{III} 2.50 V (∼2.1 V), and V^{IV}/V^{III} 2.90 V (∼3.4 V) *vs.* Na/Na^+, respectively. The mechanism of Na extraction from $Na_4Ti^{III}V^{II}(PO_4)_3$ has been shown to occur *via* a solid-solution mechanism for the V^{III}/V^{II} redox couple, followed by a two-phase reaction for both the Ti^{IV}/Ti^{III} and V^{IV}/V^{III} redox couples.[48]

Due to the existence of multiple voltage steps in $Na_xMM'(PO_4)_3$ (where M′ = Ti, V, Cr, Mn, Fe, Co and Ni and M = Ti), we directly compare the computed average voltage per Na^+ exchanged over the entire composition range (*i.e.*, $1 \leq x \leq 4$), as shown in Fig. 5. Importantly, the overall average voltage monotonically increases from Ti to Ni in cases where M = M′ and M = Ti, which is consistent with trends in standard reduction potentials of the transition metals. We note that the M^{4+} ions, in particular, become more oxidizing as one crosses the transition series from Ti to Ni, with the lack of voltage increase from Mn to Fe reflecting the stability of their $3d^5$ configurations. Specifically, the calculated voltages increase from ∼1.96 V (for Ti) to ∼4.40 V *vs.* Na/Na^+ (for Ni) in $Na_xM_2(PO_4)_3$ (green line in Fig. 5), while the maximum voltage is ∼3.73 V for Ti–Ni in the case of $Na_xMM'(PO_4)_3$ (M = Ti) systems (orange line). Notably, the voltage values for $Na_xTiM'(PO_4)_3$ are consistently lower than those for the corresponding $Na_xM'_2(PO_4)_3$, indicating that replacing Ti with another 3d metal will always lead to an increased average voltage in both M = M′ and Ti–M′ systems.

2.4 Intercalation voltages of $Na_xMM'(PO_4)_3$

Fig. 6 consolidates the computed voltages of 28 plausible combinations of 3d TMs in $Na_xMM'(PO_4)_3$ with M and M′ in a 1 : 1 ratio. In Fig. 6, the boxes outlined in red represent the

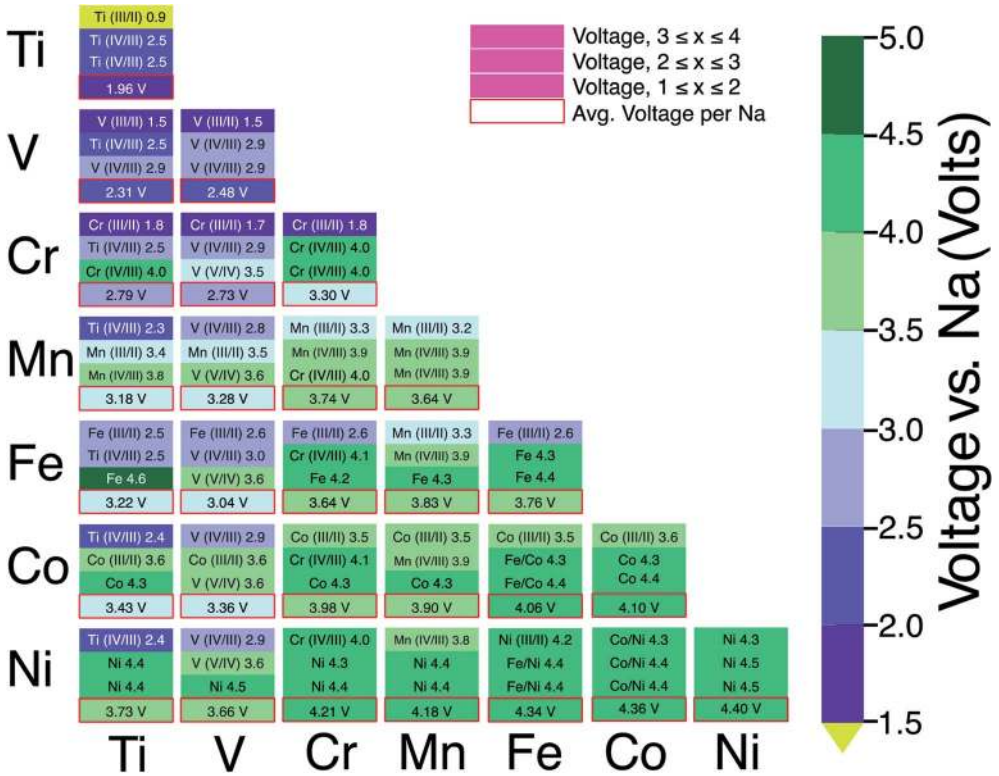

Fig. 6 A voltage map derived from our calculations of 3d NaSICON electrodes, $Na_xMM'(PO_4)_3$, where M and M′ = Ti, V, Cr, Mn, Fe, Co and Ni. The text in each box represents the redox pair and the corresponding voltage *vs.* Na/Na^+ (given by the color bar). The color of the text in the sub-boxes (black or white) does not have any physical significance other than to enhance the visibility of the plot. The color fill in each sub-box represents the voltage from the scale given on the right. The red-outlined bottom sub-box reflects the average voltage per Na in the overall range of $1 \leq x \leq 4$.

average voltage per extracted Na in the entire $1 \leq x \leq 4$ concentration range for each combination of TM. The NaSICON systems investigated cover a range of average voltages from ~1.96 to ~4.4 V *vs.* Na/Na^+. Redox couples are indicated in each box whenever we could identify the appropriate oxidation states as described in Section 2.2. The diagonal of Fig. 6 displays the single-TM NaSICONs (M = M′), whose average voltages map directly to Fig. 5. Notably, the highest average voltages of ~4.3 to 4.4 V are attained by the theoretical $Na_xNi_2(PO_4)_3$, Na_x-$CoNi(PO_4)_3$ and $Na_xFeNi(PO_4)_3$ compounds. In general, voltages in NaSICONs are set by the redox couples M^{III}/M^{II} and M^{IV}/M^{III} but notable exceptions to this trend are for V and Nb-based

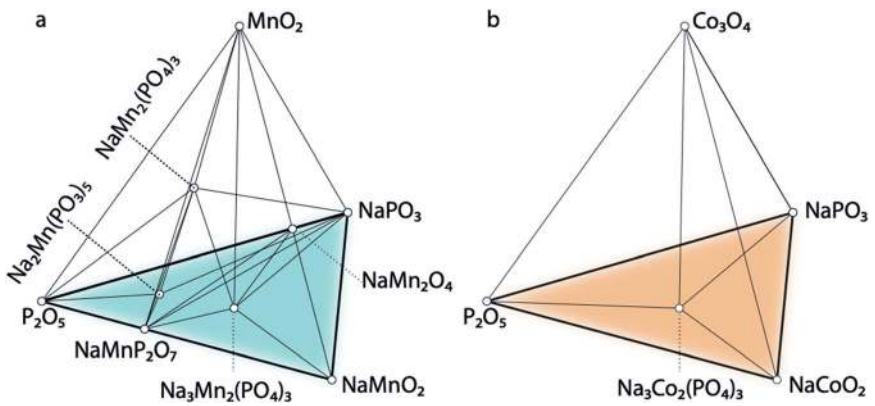

Fig. 7 Panels (a) and (b) show portions of the computed phase diagrams of Na–P–O–Mn and Na–P–O–Co at 0 K. Two stable NaSICON structures, *i.e.*, $NaMn_2(PO_4)_3$ and $Na_3Mn_2(PO_4)_3$, are observed in the phase diagram of Na–P–O–Mn, which are in equilibrium with the highly stable binary (P_2O_5 and MnO_2) and ternary ($NaMnO_2$ and $NaPO_3$) compounds. In panel (b), a stable NaSICON structure, *i.e.*, $Na_3Co_2(PO_4)_3$, is observed in the phase diagram of Na–P–O–Co, which is in equilibrium with the highly stable binary (P_2O_5 and Co_3O_4) and ternary ($NaCoO_2$ and $NaPO_3$) compounds.

NaSICONs, which can also operate on the V^{V}/V^{IV} couple (see the mixed $Na_xVM'(PO_4)_3$ systems in Fig. 6) and the Nb^{V}/Nb^{IV} couple in $Na_xNbTi(PO_4)_3$ not discussed here.[65]

2.5 Thermodynamic stabilities of selected $Na_xM_2(PO_4)_3$ compounds

The calculated quaternary phase diagrams for the systems Na–P–O–Mn, Na–P–O–Co, and Na–P–O–Ni (Fig. 7 and S34 in the ESI†) reflect the stabilities of the unreported NaSICONs with these transition metals compared with the stable elemental, binary, ternary and quaternary phases. While it remains extremely challenging to characterize quaternary (and beyond) phase diagrams solely based on sparse experimental data, theory provides a viable alternative for investigating such complex systems. We calculated all the binary/ternary/quaternary compounds available in the inorganic crystal structure database (ICSD)[66] within the Na–P–O–Mn, –Co and –Ni quaternary systems.

Fig. 7a shows the computed phase diagram of the Na–P–O–Mn system, where open circles correspond to stable phases in the global phase diagrams and the black lines show the equilibria among various compounds. The computed phase diagram of Na–Mn–P–O shows that $Na_3Mn^{III}Mn^{III}(PO_4)_3$ and $Na_1Mn^{IV}Mn^{IV}(PO_4)_3$ are stable compounds. $Na_3Mn^{III}Mn^{III}(PO_4)_3$ has the structure of the monoclinic (*Cc*) polymorph, whereas $Na_1Mn^{IV}Mn^{IV}(PO_4)_3$ has a rhombohedral ($R\bar{3}$) structure. From our computations, we observed a Jahn–Teller distortion driven by the Mn^{3+} $3d^4$ ions and highlighted by four longer equatorial bonds of ~2.10 Å and two shorter axial bonds of ~1.96 Å. No Ni-containing NaSICON phases appear stable in the Na–Ni–P–O system (Fig. S34†). In the Na–Co–P–O phase diagram (Fig. 7b), only $Na_3Co^{III}Co^{III}(PO_4)_3$ appears stable and exhibits rhombohedral symmetry ($R\bar{3}$). From this analysis, it is predicted that $Na_3Mn^{III}Mn^{III}(PO_4)_3$, $Na_1Mn^{IV}Mn^{IV}(PO_4)_3$, and $Na_3Co^{III}Co^{III}(PO_4)_3$ have the potential for successful experimental synthesis, given their thermodynamic stabilities.

Table 1 Experimentally observed $Na_xMM'(PO_4)_3$ phases along with the corresponding Na concentrations, structures, Na^+ reversible intercalation voltages, redox couples, mechanism of Na^+ intercalation, and gravimetric capacities. The intercalation voltages (in V) and theoretical (Theo.) capacities (in mA h g^{-1}) are shown. Rev. and Irrev. indicate experimentally reversible and irreversible processes. ? is used whenever the space group of a specific phase is unknown or not reported. Intercalation voltages account for the number of Na^+ ions exchanged. Whenever available, the space group of each phase is reported. For a transparent comparison between theoretical and experimentally reported capacities, the reported capacities are renormalized to the molecular weight of $Na_4MM'(PO_3)_4$. The theoretical capacities (Theo.) are also computed with respect to the $Na_4MM'(PO_3)_4$ compound

M = M′	$x = 1$	2	3	4	Reported capacity	Theo. capacity
Ti–Ti[28]	?		$P\bar{1}$	$R\bar{3}c$	142.7	170.1
		2.1 V, Ti^{IV}/TI^{III}, Rev.	0.4 V, Ti^{III}/TI^{II}, Irrev.			
V–V[37,39]	$R\bar{3}c$		$C2/c$	$R\bar{3}c$	156.7	167.9
		3.4 V, V^{V}/V^{III}, Rev.	1.6 V, V^{III}/V^{II}, Irrev.			
Cr–Cr[45]	$R\bar{3}c$		$R\bar{3}c$		93.3	111.5
		4.5 V, Cr^{IV}/Cr^{III}, Rev.				
Fe–Fe[43,44]	?		$C2/c$	$R\bar{3}c$	85.8	164.6
		3.4 V, Fe^{IV}/Fe^{III}, Rev.	2.5 V, Fe^{III}/Fe^{II}, Rev.			

M–M′	$x = 1$	2	3	4	Reported capacity	Theo. capacity
Ti–V[48,49]	$R\bar{3}c$	$R\bar{3}c$	$C2/c$	$R\bar{3}c$	132.8	169.0
	3.4 V, V^{IV}/V^{III}, Rev.	2.1 V, Ti^{IV}/TI^{III}, Rev.	1.6 V, V^{III}/V^{II}, Rev.			
Ti–Cr[52]	$R\bar{3}c$	$R\bar{3}c$	$R\bar{3}c$		—	112.4
	4.5 V, Cr^{IV}/Cr^{III}, Rev.	2.1 V, Ti^{IV}/TI^{III}, Rev.				
Ti–Mn[50,51]	$R\bar{3}c$	$R\bar{3}c$	$R\bar{3}c$	?	152.3	167.6
	4. V, Mn^{IV}/Mn^{III}, Rev.	3.5 V, Mn^{III}/Mn^{II}, Rev.	2.1 V, Ti^{IV}/TI^{III}, Rev.			
Ti–Fe[52]		$R\bar{3}c$	$R\bar{3}c$	$R\bar{3}c$	—	111.5
		2.4 V, Fe^{III}/Fe^{II}, Rev.	2.1 V, Ti^{IV}/TI^{III}, Rev.			
V–Cr[47]	?	?	$R\bar{3}$c		85.7	111.7
	4.1 V, V^{V}/V^{IV}, Rev.	3.4 V, V^{IV}/V^{III}, Rev.				
V–Mn[34,54,56]	$R\bar{3}c$	$R\bar{3}c$	$R\bar{3}c$	$R\bar{3}c$	156.0	166.6
	3.9 V, V^{V}/V^{IV}, Irrev.	3.6 V, Mn^{III}/Mn^{II}, Rev.	3.4 V, VI^{V}/V^{III}, Rev.			
V–Fe[29,35]		?	$C2/c$	?	98.1	110.8
		3.3 V, V^{IV}/V^{III}, Rev.	2.5 V, Fe^{III}/Fe^{II}, Rev.			
V–Ni[35]		?	?	$R\bar{3}c$	80.0	110.2
		3.9 V,V^{V}/V^{IV} : Ni^{III}/Ni^{II}, Rev.	3.5 V, V^{IV}/V^{III}, Rev.			
Cr–Mn[30,46]	$R\bar{3}c$	$R\bar{3}c$	$R\bar{3}c$	$R\bar{3}c$	160.5	166.2
	4.4 V, Cr^{IV}/Cr^{III}, Rev.	4.2 V, Mn^{IV}/Mn^{III}, Rev.	3.6 V, Mn^{III}/Mn^{II}, Rev.			

3. Discussion

Using first-principles calculations, we investigated the electrochemical properties of 28 transition-metal-based NaSICONs as cathode materials for NIBs. To guide our discussion, we summarize the reported experimental voltages and the experimental gravimetric and the theoretical gravimetric capacities of some $Na_xMM'(PO_4)_3$ systems in Table 1. For a transparent and fair comparison between the theoretical and experimentally reported capacities in Table 1, the reported capacities are renormalized from the reported composition (pristine) to the molecular weight of the $Na_4MM'(PO_3)_4$. The theoretical capacities are also computed with respect to the $Na_4MM'(PO_3)_4$ compounds.

Among the $Na_xM_2(PO_4)_3$ compounds, $Na_xCr_2(PO_4)_3$ delivers the highest measured voltage of ~4.5 V (~4 V calculated theoretically) *vs.* Na/Na^+,[45] albeit with a limited capacity of just ~98 mA h g^{-1} and corresponding to the extraction of 2 Na from $Na_3Cr^{III}Cr^{III}(PO_4)_3$ to form $Na_1Cr^{IV}Cr^{III}(PO_4)_3$. $Na_4Cr_2(PO_4)_3$ has not yet been obtained by either a chemical or an electrochemical process. $Na_4Cr^{III}Cr^{II}(PO_4)_3$ would require Cr to exist in a mixed, Cr^{III}/Cr^{II} oxidation state, with Cr^{2+} (high-spin d^4) typically being an unstable oxidation state for Cr and easily prone to Jahn–Teller distortions in octahedral environments, *e.g.*, NaSICON.[67]

$Na_xV_2(PO_4)_3$ exhibits the 2nd highest measured voltage of the single TM NaSICONs, with a computed average voltage of ~2.48 V *vs.* Na/Na^+ (Fig. 5). With the same number of maximum electrons exchanged in $Na_xM_2(PO_4)_3$ (where M = Ti or V), and Ti being lighter than V, $Na_xTi_2(PO_4)_3$ is expected to show the largest gravimetric capacity. $Na_xTi_2(PO_4)_3$ and NVP provide the largest reported theoretical gravimetric capacities (~170.1 mA h g^{-1} and ~167.9 mA h g^{-1} for $Na_4M_2(PO_4)_3$) in single TM NaSICONs. In theory, additional capacity and an increased voltage could be achieved by exploiting the V^V/V^{IV} redox couple in the reaction $Na_1V^{IV}V^{IV}(PO_4)_3 \rightarrow Na^+ + 1e^- V^VV^{IV}(PO_4)_3$. While the seminal report by Gopalakrishnan *et al.* suggested the possibility of chemically extracting the last Na^+ ion to form $V^VV^{IV}(PO_4)_3$,[68] subsequent attempts to do so have proven unsuccessful. Note that $V^VV^{IV}(PO_4)_3$ is not a thermodynamically stable compound[69] and is predicted to decompose into $VPO_5 + VP_2O_7$.

We assessed the existence of uncharted single-TM NaSICONs, which are Ni, Co and Mn. Except for $Na_1Mn^{IV}Mn^{IV}(PO_4)_3$, $Na_3Mn^{III}Mn^{III}(PO_4)_3$ and $Na_3Co^{III}Co^{III}(PO_4)_3$ that appear stable according to our convex hulls but have not been reported experimentally, our analysis of the phase diagrams indicates that Ni- and Co-NaSICONs are generally unstable. However, Mn has been mixed effectively with Ti, V and Cr, while Ni–V mixed NaSICONs have also been made (Table 1).[34] In particular, Zhou *et al.*[35] and later Chen and collaborators[34] synthesized Mn^{II}-containing $Na_4Mn^{II}V^{III}(PO_4)_3$, which upon Na extraction exploits the Mn^{III}/Mn^{II} redox couple and Mn^{3+} $3d^4$ is Jahn–Teller active.

In the case of mixed $Na_4MM'(PO_4)_3$ NaSICONs, we kept the M : M′ ratio to 1 : 1. From an extensive assessment of polyanion electrodes, Masquelier and Croguennec[17] observed that the redox potentials of specific TMs remain nearly independent[70] of those of other TMs that may be present. This general rule is also well supported by the simulations that are summarized in Fig. 6. Based on this general principle, one can envision selected combinations of TMs delivering reversible high voltages *vs.* Na/Na^+. For example, the Ti^{IV}/Ti^{III} redox couple showed a similar voltage[17] (~2.1 V *vs.* Na/Na^+) in three related NaSICON systems: $Na_xTi_2(PO_4)_3$, $Na_xTiNb(PO_4)_3$ and $Na_xTiFe(PO_4)_3$. Notably, in experiments, there is a consistent shift of ~0.3 V between the voltages measured *vs.* Na/Na^+ compared to those measured *vs.* Li/Li^+.

The $Na_xTiV(PO_4)_3$ system has been shown to provide the largest gravimetric capacity (~187.1 mA h g^{-1}, Table 1) among NaSICONs as a result of the accessibility of several $V^{IV}/V^{III}/V^{II}$ and Ti^{IV}/Ti^{III} redox couples. Nevertheless, the computed average voltage (~2.3 V, Fig. 6) of $Na_xTiV(PO_4)_3$ highlights the low energy density of the system.[48,49] More promising in terms of overall capacities and voltages, and thus energy density, are $Na_xTiCr(PO_4)_3$,[52,64] $Na_xTiMn(PO_4)_3$,[50,51] $Na_xCrMn(PO_4)_3$,[30,46] $Na_xVCr(PO_4)_3$,[47] and $Na_xVMn(PO_4)_3$,[34,54] but the reversible extraction/insertion of Na from some of these systems remains to be verified. Excluding some specific exceptions, especially Fe, Co and Ni based NaSICONs since they appear metallic, our simulations are also able to capture the mechanism of Na intercalation in mixed NaSICON electrodes. For example, $Na_3VFe(PO_4)_3$ has been reported to reversibly insert Na with the activation of the Fe^{III}/Fe^{II} and V^{III}/V^{II} redox couples (see Table 1),[35] and this behavior is reproduced by our calculations (Fig. 6 and S21 of the ESI†). Similar conclusions can be advanced for mixed TiV, TiCr, VCr and CrMn NaSICON materials.

From our analysis (Fig. 6), specific unexplored combinations of TMs appear to be worthy of future study. Our calculations suggest promising NaSICON compositions in terms of average voltages, such as TiCo, VCo, CrFe and CrCo NaSICONs as reported in Fig. 5 and Table 1. Both CrFe and CrCo NaSICONs are predicted to exploit the high voltage Cr^{IV}/Cr^{III} redox couple, which has been proven effective in other mixed NaSICONs, *e.g.*, TiCr, VCr and MnCr.[47,64] Although the addition of Co into Ti, V and Cr appears interesting, our analysis of the $Na_xCo_2(PO_4)_3$ system suggests that only $Na_3Co^{III}Co^{III}(PO_4)_3$ with Co^{3+} $3d^6$ (low spin) is thermodynamically stable, but this compound has not yet been synthesized. While one would target compounds with Co^{2+} to ensure high voltages, it appears possible to introduce Co in smaller proportions[71] than a 1 : 1 ratio, but more experimental and theoretical work is required.

We do not anticipate Ni to be of importance in mixed NaSICON systems due to the high instability of quaternary $Na_xNi_2(PO_4)_3$. Manoun *et al.*[72] briefly reported the synthesis of $Na_4Cr^{III}Ni^{II}(PO_4)_3$. A recent report by Zhou *et al.*[35] claimed the extraction of Na from $Na_xVNi(PO_4)_3$ (Table 1) involving the redox couples V^{IV}/V^{III}, V^V/V^{IV}, and Ni^{III}/Ni^{II}. Nevertheless, we speculate that the Ni content of the materials is not in a 1 : 1 ratio but appears to be significantly lower. Furthermore, the highest voltage accessed (<4.3 V *vs.* Na/Na^+) during the electrochemical cycling is lower than that of the expected Ni redox couple. While our DFT calculations seem to verify the activity of the V^{IV}/V^{III} and V^V/V^{IV} redox couples in $Na_xVNi(PO_4)_3$ (Fig. 6), we are unable to verify the oxidation states involved in the

Ni^{III}/Ni^{II} reaction from the computed magnetic moments as the material becomes metallic in our simulations (Fig. S12†). Our findings also cast doubt on the activity of Ni in this compound as reflected by the limited gravimetric capacity reported experimentally (~80 mA h g^{-1}).[35]

4. Conclusions

Using *ab initio* density functional theory and thermodynamics, we explored the full chemical map of 3d TM-based NaSICON phosphate $Na_xMM'(PO_4)_3$ (M, M′ = Ti, V, Cr, Mn, Fe, Co and Ni) cathode materials for high-energy density and safe sodium-ion batteries. We identified the ground state structures at various Na contents as well as the corresponding Na-intercalation voltages and redox processes for 28 distinct NaSICON compositions of which only 13 have been reported experimentally.

Further, we investigated the Na-intercalation properties of previously unreported $Na_xMn_2(PO_4)_3$ and $Na_xVCo(PO_4)_3$ ($1 \leq x \leq 4$), among others. The calculated quaternary phase diagrams of the Na–P–O–M (M = Mn, Co and Ni) chemical systems indicate the instability of Ni and most Co-based NaSICONs, though the $Na_1Mn^{IV}Mn^{IV}(PO_4)_3$, $Na_3Mn^{III}Mn^{III}(PO_4)_3$ and $Na_3Co^{III}Co^{III}(PO_4)_3$ compounds are identified as stable compositions. We performed a complete analysis of the wide-ranging chemical space of NaSICON phosphate cathode materials for Na-ion batteries, and our work can be used to guide further experimental synthesis of the new and promising compositions identified here. We plan to synthesize the promising electrode compositions identified in this work.

5. Methodology

We used the Vienna *ab initio* simulation package (VASP)[73,74] for *ab initio* density functional theory (DFT) total energy calculations. The projector augmented wave (PAW) potentials were used for the core wave-functions. The Perdew–Burke–Ernzerhof (PBE) parameterized spin-polarized generalized gradient approximation (GGA) was used for the exchange and correlation energy.[75] The strong on-site coulomb correlation of 3d electrons of the TM (Ti, V, Cr, Mn, Fe, Co and Ni) is addressed with Hubbard's U correction[76] according to the Dudarev method.[77] The effective U parameters used were 4.0 eV for Ti,[28] 3.1 for V, 3.5 for Cr, 3.9 for Mn, 4.0 for Fe, 3.4 for Co, and 6.0 for Ni,[78] and they were fitted to match the experimental formation energies of binary oxides. We also introduced an empirical correction of 1.36 eV per O_2 (ref. 79) to remedy the spurious error originating from the well-known over-binding of O while using GGA.

The periodic wave functions were expanded in terms of plane waves up to a kinetic energy cut-off of 520 eV. The PAW potentials used to describe the core electrons of the following atomic species were: Na 08Apr2002 $3s^1$, P 17Jan2003 $2s^23p^3$, O 08Apr2002 $2s^22p^4$, Ti 08Apr2002 $3d^34s^1$, V_pv 07Sep2000 $3p^63d^44s^1$, Cr 06Sep2000 $3d^54s^1$, Mn 06Sep2000 $3d^64s^1$, Fe 06Sep2000 $3d^74s^1$, Co 06Sep2000 $3d^84s^1$, and Ni 06Sep2000 $3d^94s^1$. Additionally, a Γ-centered Monkhorst–Pack[80] k-point mesh with 25 subdivisions along each reciprocal lattice vector was applied to all structures. Using these settings, the total energy of each structure was converged to within 10^{-5} eV per cell, atomic forces within 10^{-2} eV per Å and the stress within 0.29 GPa.

An intercalation battery based on the NaSICON cathode electrodes implies the reversible insertion/extraction of Na^+-ions into/from the $Na_yMM'(PO_4)_3$ framework according to the redox reaction of eqn (1).

$$Na_yMM'(PO_4)_3 + (x-y)Na^+ + (x-y)e^- \xleftrightarrow{-\Delta G^0} Na_xMM'(PO_4)_3 \quad (1)$$

where y and x are the initial and final Na concentration in the NaSICON framework and ΔG^0 is the change of Gibbs energy at 0 K for the reaction of eqn (1). Here, we approximated the Gibbs energy of each component by the DFT total energies (*i.e.*, $G \approx E$), thus neglecting the pV and entropic contributions. The average voltage across an intercalation extent $(x - y)$ can be calculated from the ΔG^0, as in eqn (2).

$$V = -\frac{\Delta G^0}{(x-y)F} = -\frac{E\left(Na_xMM'(PO_4)_3\right) - \left[E\left(Na_yMM'(PO_4)_3\right) + (x-y)\mu_{Na}\right]}{(x-y)F} \quad (2)$$

where μ_{Na} is the Na chemical potential (set to bulk Na metal) and F is the Faraday constant.

To establish the general phase behavior of Na (de)intercalation into the $Na_yMM'(PO_4)_3$ structure, we monitored, using eqn (3), the formation energies ($E_f(x)$) of various Na/vacancy orderings at different Na concentrations, x ($1 \leq x \leq 4$), with respect to the DFT energies of the fully discharged (*i.e.*, $E[Na_4MM'(PO_4)_3]$) and fully charged ($E[NaMM'(PO_4)_3]$) configurations.

$$E_f(x) = E\left[Na_xMM'(PO_4)_3\right] - \left(\frac{4-x}{3}\right)E\left[Na_1MM'(PO_4)_3\right] - \left(\frac{x-1}{3}\right)E\left[Na_4MM'(PO_4)_3\right]. \quad (3)$$

Different NaSICON structures were studied according to specific Na concentrations in $Na_xMM'(PO_4)_3$ with M and M′ = Ti, V, Cr, Mn, Fe, Co, and Ni. In choosing the amount of mixing of TM in these NaSICON structures, we have considered only two distinct situations: (i) M = M′, which leads to $Na_xM_2(PO_4)_3$, and (ii) M and M′ in the ratio 1 : 1.

When fully sodiated, the fully ordered rhombohedral symmetry ($R\bar{3}c$) of the high temperature NaSICON structure is typically observed (*e.g.*, $Na_4Fe^{III}Fe^{II}(PO_4)_3$ (ref. 59)) and is therefore our starting model to study Na removal and TM mixing. Na vacancies are created in the fully sodiated structure $Na_4MM'(PO_4)_3$, resulting in $Na_xMM'(PO_4)_3$, where the Na content varies in the range of $1 \leq x \leq 4$ in steps of $\Delta x = 0.5$. The possible configurations originating from the various orderings of Na and vacancies (Va) in the NaSICON are obtained using the pymatgen library.[81] A ranking according to the classical Ewald energy[82] based on integer charges (*i.e.*, Na = +1, P = +5, O = −2)

and the variable charge on the TM (+2, +3 and +4) is applied to limit the number of possible structures to a computationally tractable level. For mixed TM NaSICONs, the ordering of M and M′ is simultaneously performed with that of Na and Va. DFT calculations are performed on the primitive cell and supercells ($2 \times 1 \times 1$) of these orderings. A formula unit of the fully discharged NaSICON ($Na_4MM'(PO_4)_3$) contains 21 atoms.

Conflicts of interest

There are no conflicts to declare.

Acknowledgements

P. C., C. M., A. K. C., and J.-N. C. are grateful to the ANR-NRF NRF2019-NRF-ANR073 Na-MASTER. P. C. and B. S. acknowledge funding from the National Research Foundation under the NRF Fellowship NRFF12-2020-0012. L. C., D. C. and C. M. acknowledge the ANRT and TIAMAT for the funding of S. P.'s PhD thesis as well as the financial support from the Région Nouvelle Aquitaine and from the French National Research Agency (STORE-EX Labex Project ANR-10-LABX-76-01). The computational work was performed using resources of the National Supercomputing Centre, Singapore (https://www.nscc.sg).

References

1 E. A. Olivetti, G. Ceder, G. G. Gaustad and X. Fu, *Joule*, 2017, **1**, 229.
2 J. M. Tarascon, *Nat. Chem.*, 2010, **2**, 510.
3 D. Larcher and J. M. Tarascon, *Nat. Chem.*, 2015, **7**, 19.
4 S. W. Kim, D. H. Seo, X. Ma, G. Ceder and K. Kang, *Adv. Energy Mater.*, 2012, **2**, 710.
5 V. Palomares, P. Serras, I. Villaluenga, K. B. Hueso, J. Carretero-González and T. Rojo, *Energy Environ. Sci.*, 2012, **5**, 5884.
6 J. L. Kaufman, J. Vinckevičiūtė, S. K. Kolli, J. G. Goiri and A. Van Der Ven, *Philos. Trans. R. Soc., A*, 2019, **377**, 20190020.
7 Q. Bai, L. Yang, H. Chen and Y. Mo, *Adv. Energy Mater.*, 2018, **8**, 1.
8 A. Mukherjee, T. Sharabani, R. Sharma, S. Okashy and M. Noked, *Batteries Supercaps*, 2020, **3**, 510.
9 N. Yabuuchi, K. Kubota, M. Dahbi and S. Komaba, *Chem. Rev.*, 2014, **114**, 11636.
10 I. Hasa, S. Mariyappan, D. Saurel, P. Adelhelm, A. Y. Koposov, C. Masquelier, L. Croguennec and M. Casas-Cabanas, *J. Power Sources*, 2021, **482**, 228872.
11 S. H. Bo, X. Li, A. J. Toumar and G. Ceder, *Chem. Mater.*, 2016, **28**, 1419.
12 J.-M. Tarascon, *Joule*, 2020, **4**, 1613–1620.
13 K. Kubota, T. Asari, H. Yoshida, N. Yaabuuchi, H. Shiiba, M. Nakayama and S. Komaba, *Adv. Funct. Mater.*, 2016, **26**, 6047.
14 P. F. Wang, Y. You, Y. X. Yin and Y. G. Guo, *Adv. Energy Mater.*, 2018, **8**, 1701912.
15 J. L. Kaufman and A. Van der Ven, *Phys. Rev. Mater.*, 2019, **3**, 015402.
16 T. Jin, H. Li, K. Zhu, P. F. Wang, P. Liu and L. Jiao, *Chem. Soc. Rev.*, 2020, **49**, 2342.
17 C. Masquelier and L. Croguennec, *Chem. Rev.*, 2013, **113**, 6552.
18 S. C. Chung, J. Ming, L. Lander, J. Lu and A. Yamada, *J. Mater. Chem. A*, 2018, **6**, 3919.
19 P. Barpanda, G. Oyama, S. Nishimura, S.-C. Chung and A. Yamada, *Nat. Commun.*, 2014, **5**, 4358.
20 H. Y. P. Hong, *Mater. Res. Bull.*, 1976, **11**, 173.
21 J. B. Goodenough, H. Y. P. Hong and J. A. Kafalas, *Mater. Res. Bull.*, 1976, **11**, 203.
22 Q. Ma, C. L. Tsai, X. K. Wei, M. Heggen, F. Tietz and J. T. S. Irvine, *J. Mater. Chem. A*, 2019, **7**, 7766.
23 Z. Jian, Y. S. Hu, X. Ji and W. Chen, *Adv. Mater.*, 2017, **29**, DOI: 10.1002/adma.201601925.
24 R. V. Panin, O. A. Drozhzhin, S. S. Fedotov, N. R. Khasanova and E. V. Antipov, *Electrochim. Acta*, 2018, **289**, 168.
25 C. Delmas, F. Cherkaoui, A. Nadiri and P. Hagenmuller, *Mater. Res. Bull.*, 1987, **22**, 631.
26 C. Delmas, A. Nadiri and J. L. Soubeyroux, *Solid State Ionics*, 1988, **28–30**, 419.
27 X. Zhang, X. Rui, D. Chen, H. Tan, D. Yang, S. Huang and Y. Yu, *Nanoscale*, 2019, **11**, 2556.
28 P. Senguttuvan, G. Rousse, M. E. Arroyo y de Dompablo, H. Vezin, J.-M. Tarascon and M. R. Palacín, *J. Am. Chem. Soc.*, 2013, **135**, 3897.
29 B. M. de Boisse, J. Ming, S. Nishimura and A. Yamada, *J. Electrochem. Soc.*, 2016, **163**, A1469.
30 J. Wang, Y. Wang, D. Seo, T. Shi, S. Chen, Y. Tian, H. Kim and G. Ceder, *Adv. Energy Mater.*, 2020, **10**, 1903968.
31 D. A. Stevens and J. R. Dahn, *J. Electrochem. Soc.*, 2000, **147**, 1271.
32 M. Dahbi, M. Kiso, K. Kubota, T. Horiba, T. Chafik, K. Hida, T. Matsuyama and S. Komaba, *J. Mater. Chem. A*, 2017, **5**, 9917.
33 H. Kim, J. Hong, G. Yoon, H. Kim, K.-Y. Park, M.-S. Park, W.-S. Yoon and K. Kang, *Energy Environ. Sci.*, 2015, **8**, 2963.
34 F. Chen, V. M. Kovrugin, R. David, O. Mentré, F. Fauth, J. Chotard and C. Masquelier, *Small Methods*, 2019, **3**, 1800218.
35 W. Zhou, L. Xue, X. Lü, H. Gao, Y. Li, S. Xin, G. Fu, Z. Cui, Y. Zhu and J. B. Goodenough, *Nano Lett.*, 2016, **16**, 7836.
36 X. Yao, Z. Zhu, Q. Li, X. Wang, X. Xu, J. Meng, W. Ren, X. Zhang, Y. Huang and L. Mai, *ACS Appl. Mater. Interfaces*, 2018, **10**, 10022.
37 K. Saravanan, C. W. Mason, A. Rudola, K. H. Wong and P. Balaya, *Adv. Energy Mater.*, 2013, **3**, 444.
38 Y. Uebou, T. KiyabuI, S. Okada and J. Yamaki, *Rep. Inst. Adv. Mater. Study, Kyushu Univ.*, 2002, **16**, 1.
39 F. Lalère, J. B. Leriche, M. Courty, S. Boulineau, V. Viallet, C. Masquelier and V. Seznec, *J. Power Sources*, 2014, **247**, 975.
40 Y. Noguchi, E. Kobayashi, L. S. Plashnitsa, S. Okada and J. I. Yamaki, *Electrochim. Acta*, 2013, **101**, 59.

41 Z. Deng, G. Sai Gautam, S. K. Kolli, J.-N. Chotard, A. K. Cheetham, C. Masquelier and P. Canepa, *Chem. Mater.*, 2020, **32**, 7908.
42 J. Kang, S. Baek, V. Mathew, J. Gim, J. Song, H. Park, E. Chae, A. K. Rai and J. Kim, *J. Mater. Chem.*, 2012, **22**, 20857.
43 Y. Liu, Y. Zhou, J. Zhang, Y. Xia, T. Chen and S. Zhang, *ACS Sustainable Chem. Eng.*, 2017, **5**, 1306.
44 R. Rajagopalan, B. Chen, Z. Zhang, X.-L. Wu, Y. Du, Y. Huang, B. Li, Y. Zong, J. Wang, G.-H. Nam, M. Sindoro, S. X. Dou, H. K. Liu and H. Zhang, *Adv. Mater.*, 2017, **29**, 1605694.
45 K. Kawai, W. Zhao, S. Nishimura and A. Yamada, *ACS Appl. Energy Mater.*, 2018, **1**, 928.
46 W. Zhang, H. Li, Z. Zhang, M. Xu, Y. Lai and S. L. Chou, *Small*, 2020, **16**, 2001524.
47 R. Liu, G. Xu, Q. Li, S. Zheng, G. Zheng, Z. Gong, Y. Li, E. Kruskop, R. Fu, Z. Chen, K. Amine and Y. Yang, *ACS Appl. Mater. Interfaces*, 2017, **9**, 43632.
48 F. Lalère, V. Seznec, M. Courty, J. N. Chotard and C. Masquelier, *J. Mater. Chem. A*, 2018, **6**, 6654.
49 D. Wang, X. Bie, Q. Fu, D. Dixon, N. Bramnik, Y. S. Hu, F. Fauth, Y. Wei, H. Ehrenberg, G. Chen and F. Du, *Nat. Commun.*, 2017, **8**, 1.
50 T. Zhu, P. Hu, X. Wang, Z. Liu, W. Luo, K. A. Owusu, W. Cao, C. Shi, J. Li, L. Zhou and L. Mai, *Adv. Energy Mater.*, 2019, **9**, 2.
51 H. Gao, Y. Li, K. Park and J. B. Goodenough, *Chem. Mater.*, 2016, **28**, 6553.
52 S. Patoux, G. Rousse, J. B. Leriche and C. Masquelier, *Chem. Mater.*, 2003, **15**, 2084.
53 H. Li, T. Jin, X. Chen, Y. Lai, Z. Zhang, W. Bao and L. Jiao, *Adv. Energy Mater.*, 2018, **8**, 1801418.
54 S. Ghosh, N. Barman, M. Mazumder, S. K. Pati, G. Rousse and P. Senguttuvan, *Adv. Energy Mater.*, 2020, **10**, 1902918.
55 M. V. Zakharkin, O. A. Drozhzhin, I. V. Tereshchenko, D. Chernyshov, A. M. Abakumov, E. V. Antipov and K. J. Stevenson, *ACS Appl. Energy Mater.*, 2018, **1**, 5842.
56 M. V. Zakharkin, O. A. Drozhzhin, S. V. Ryazantsev, D. Chernyshov, M. A. Kirsanova, I. V. Mikheev, E. M. Pazhetnov, E. V. Antipov and K. J. Stevenson, *J. Power Sources*, 2020, **470**, 228231.
57 J. N. Chotard, G. Rousse, R. David, O. Mentré, M. Courty and C. Masquelier, *Chem. Mater.*, 2015, **27**, 5982.
58 H. Kabbour, D. Coillot, M. Colmont, C. Masquelier and O. Mentré, *J. Am. Chem. Soc.*, 2011, **133**, 11900.
59 F. Hatert, *Acta Crystallogr., Sect. E: Struct. Rep. Online*, 2009, **65**, i30.
60 F. Lalère, V. Seznec, M. Courty, R. David, J. N. Chotard and C. Masquelier, *J. Mater. Chem. A*, 2015, **3**, 16198.
61 Z. Jian, C. Yuan, W. Han, X. Lu, L. Gu, X. Xi, Y. S. Hu, H. Li, W. Chen, D. Chen, Y. Ikuhara and L. Chen, *Adv. Funct. Mater.*, 2014, **24**, 4265.
62 D. Gryaznov, S. K. Stauffer, E. A. Kotomin and L. Vilčiauskas, *Phys. Chem. Chem. Phys.*, 2020, **22**, 11861.
63 M. K. Y. Chan and G. Ceder, *Phys. Rev. Lett.*, 2010, **105**, 196403.
64 J. Zhang, G. Liang, C. Wang, C. Lin, J. Chen, Z. Zhang and X. S. Zhao, *ACS Appl. Mater. Interfaces*, 2020, **12**(25), 28313–28319.
65 O. Tillement, J. C. Couturier, J. Angenault and M. Quarton, *Solid State Ionics*, 1991, **48**, 249.
66 G. Bergerhoff, R. Hundt, R. Sievers and I. D. Brown, *J. Chem. Inf. Comput. Sci.*, 1983, **23**, 66.
67 P. A. Cox, *Transition Metal Oxides: An Introduction to Their Electronic Structure and Properties*, Oxford Univeristy Press, Oxford, UK, 2010.
68 J. Gopalakrishnan and K. K. Rangan, *Chem. Mater.*, 1992, **4**, 745.
69 A. Jain, S. P. Ong, G. Hautier, W. Chen, W. D. Richards, S. Dacek, S. Cholia, D. Gunter, D. Skinner, G. Ceder and K. A. Persson, *APL Mater.*, 2013, **1**, 011002.
70 A. K. Padhi, K. S. Nanjundaswamy, C. Masquelier and J. B. Goodenough, *J. Electrochem. Soc.*, 1997, **144**, 2581.
71 H. Wang, C. Chen, C. Qian, C. Liang and Z. Lin, *RSC Adv.*, 2017, **7**, 33273.
72 B. Manoun, A. El Jazouli, S. Krimi and A. Lachgar, *Powder Diffr.*, 2004, **19**, 162.
73 G. Kresse and J. Furthmüller, *Phys. Rev. B: Condens. Matter Mater. Phys.*, 1996, **54**, 11169.
74 G. Kresse and J. Furthmüller, *Comput. Mater. Sci.*, 1996, **6**, 15.
75 J. P. Perdew, K. Burke and M. Ernzerhof, *Phys. Rev. Lett.*, 1996, **77**, 3865.
76 M. Cococcioni and S. De Gironcoli, *Phys. Rev. B: Condens. Matter Mater. Phys.*, 2005, **71**, 035105.
77 S. Dudarev and G. Botton, *Phys. Rev. B: Condens. Matter Mater. Phys.*, 1998, **57**, 1505.
78 A. Jain, G. Hautier, C. J. Moore, S. Ping Ong, C. C. Fischer, T. Mueller, K. A. Persson and G. Ceder, *Comput. Mater. Sci.*, 2011, **50**, 2295.
79 L. Wang, T. Maxisch and G. Ceder, *Phys. Rev. B: Condens. Matter Mater. Phys.*, 2006, **73**, 195107.
80 J. D. Pack and H. J. Monkhorst, *Phys. Rev. B: Solid State*, 1977, **16**, 1748.
81 S. P. Ong, W. D. Richards, A. Jain, G. Hautier, M. Kocher, S. Cholia, D. Gunter, V. L. Chevrier, K. A. Persson and G. Ceder, *Comput. Mater. Sci.*, 2013, **68**, 314.
82 P. P. Ewald, *Ann. Phys.*, 1921, **369**, 253.

